

Experimental and analytical study on shear mechanism of rubber-ring perfobond connector

Liu, Yangqing; Xin, Haohui; Liu, Yuqing

DOI

[10.1016/j.engstruct.2019.109382](https://doi.org/10.1016/j.engstruct.2019.109382)

Publication date

2019

Document Version

Final published version

Published in

Engineering Structures

Citation (APA)

Liu, Y., Xin, H., & Liu, Y. (2019). Experimental and analytical study on shear mechanism of rubber-ring perfobond connector. *Engineering Structures*, 197, Article 109382. <https://doi.org/10.1016/j.engstruct.2019.109382>

Important note

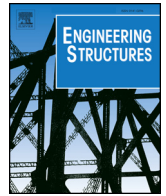
To cite this publication, please use the final published version (if applicable). Please check the document version above.

Copyright

Other than for strictly personal use, it is not permitted to download, forward or distribute the text or part of it, without the consent of the author(s) and/or copyright holder(s), unless the work is under an open content license such as Creative Commons.

Takedown policy

Please contact us and provide details if you believe this document breaches copyrights. We will remove access to the work immediately and investigate your claim.



Experimental and analytical study on shear mechanism of rubber-ring perfobond connector

Yangqing Liu^a, Haohui Xin^{a,b}, Yuqing Liu^{a,*}

^a Department of Bridge Engineering, Tongji University, Shanghai, China

^b Faculty of Civil Engineering and Geosciences, Delft University of Technology, Netherlands

ARTICLE INFO

Keywords:

Composite bridges
Perfobond connectors
Rubber
Modified push-out test
Finite element analysis
Shear behavior

ABSTRACT

This paper proposed an easy-installed rubber-ring perfobond connector (RPBL) to mitigate the shear concentration of partial holes in perfobond connector (PBL) groups. Four modified push-out tests with different rubber ring thicknesses were conducted to investigate the shear behavior of RPBLs. The test results showed that specimens experienced four stages, including (i) damage of bond, (ii) shear fractures of concrete dowels, (iii) tension-shear yielding of perforated rebars, and (iv) hardening and fractures of perforated rebars. The rubber rings can significantly improve the slip capacity and drop the shear stiffness of perfobond connectors. Compared with ordinary perfobond connectors, the yield slips of specimens with 2 mm, 4 mm and 6 mm thick rubber rings increase by 304%, 509% and 745%. Further, three-dimensional nonlinear parametric FEA (finite element analysis) models of modified push-out tests were established and verified by the test results. The shear mechanism of each component and the effects of rubber ring thickness on shear behaviors were discussed. Finally, the shear yield load equations and shear capacity equations of PBL and RPBL were proposed based on the collected modified push-out test results. The calculated results agree well with the test results.

1. Introduction

Perfobond connectors (PBL) can efficiently transfer loads between steel and concrete components with the benefits of easy installation, excellent shear behavior and fatigue performance [1]. Recently the application of PBLs has increased in composite bridges, such as interfaces of composite girders, hybrid girder joints, hybrid truss joints, anchorage zones of composite pylons and anchorage joints between suspenders and girders [2]. To guarantee sufficient shear resistance in composite structures, PBLs are usually in an arrangement of multiple rows and columns.

However, as shown in Fig. 1(a), part of the PBLs in the connector group have been in the plastic state although the average shear force is still below the shear carrying capacity of an individual connector. The shear concentration of PBLs in multi rows and columns will lead to unsafe design. Oguejiofor et al. [3] found that the shear capacity did not increase with the number of rib holes when the hole spacing was less than 2.25 times the hole diameter. This indicates that the interactions between adjacent holes exist. Ahn et al. [5] carried out push-out tests of twin PBLs, i.e., the two ribs arranged side by side. The test results show that the shear capacity is 80% that of the single rib since the contributions of concrete end-bearing zones, concrete dowels and

perforated rebars reduce. Su et al. [11] compared the shear capacity of single-hole specimens with two-hole specimens and concluded a reduction factor of about 0.9, demonstrating the shear capacity of every single hole cannot be fully realized. Zhang et al. [18] conducted experimental studies on PBL groups and discussed non-uniform load distribution in groups. The unevenness factor exceeds 2 at serviceability stage when more than eight layers are employed. Also, Liu et al. [2] carried out model tests, numerical simulation and theoretical analysis to investigate the load transfer mechanism of PBLs in suspender-girder composite anchorage joints. The PBLs in the first row undertook about one-third of the applied load in the serviceability stage. Overall, the shear concentration in PBL groups is prominent. Neglecting the possible adverse effects induced by shear concentration may produce unconservative design.

To alleviate local shear concentration in groups, a possible solution is diminishing the initial shear stiffness of PBLs. Xu et al. [20,21] reduced the initial shear stiffness of headed shear studs by using rubber sleeves which are much softer than concrete and steel. The rubber sleeves reduce the contact area between the studs and the concrete blocks, so that the initial stiffness of studs is lower at early loading stages. Based on this concept, the authors proposed the rubber ring which consists of an inner ring and two side wings, as shown in Fig. 2,

* Corresponding author.

E-mail address: yql@tongji.edu.cn (Y. Liu).

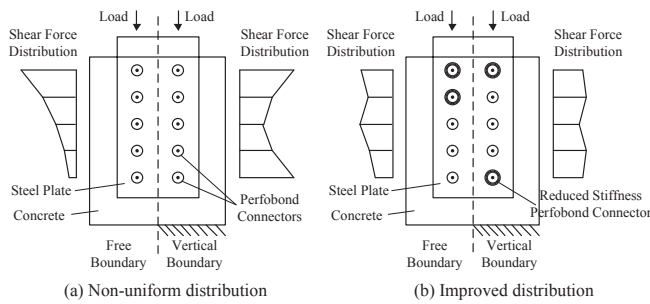


Fig. 1. Shear distributions in perfobond connector groups.

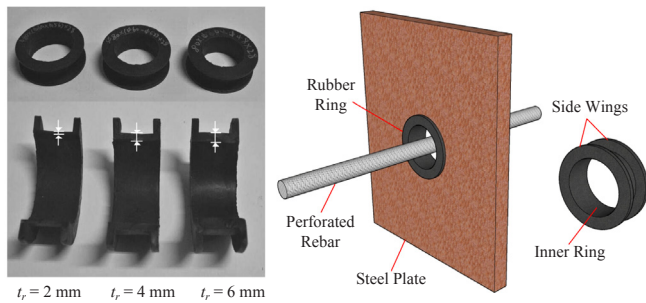


Fig. 2. Rubber rings and specimen assembly.

to decrease the initial shear stiffness of PBLs. By setting rubber rings to partial PBLs in groups, the shear distribution will tend to be uniform, as shown in Fig. 1(b).

In the past two decades, researchers investigated the shear behavior of PBLs by push-out tests and numerical simulations and put forward shear capacity equations based upon regression analysis and neural network [3–7]. The ordinary push-out test is suitable for the shear connectors applied to the interfaces of composite girders. However, positions of PBLs and dimensions of concrete blocks in composite joints are entirely different from those in composite girders. Yamadera et al. [8] proposed and carried out a modified push-out test in which the PBLs were embedded in massive concrete blocks. Then Wang et al. [9] and Su et al. [10,11] summarized failure modes and appropriate application situations of ordinary and modified push-out tests. In modified push-out tests, concrete splitting cracks and crushing are prevented by the large volume of concrete, leading that the shear force keeps increasing till the ultimate shear capacity. As PBLs are increasingly used in hybrid structures and anchorage joints, the effects of hole diameter, perforated rebar diameter, the bond between steel and concrete, steel plate thickness and concrete strength on the shear performance were researched by modified push-out tests [12–19]. Although a number of studies on shear behavior of PBLs had been conducted, the works about improving shear distribution in PBL groups are limited as far as authors’ knowledge. Thus it is significant to investigate the shear behavior and application possibilities of RPBLs which can alleviate local shear concentration in PBL groups.

In this paper, modified push-out tests were conducted to study the shear behavior of RPBLs. The experimental parameter investigated is the thickness of rubber rings. The failure modes, load-slip curves, strains on steel plates and perforated rebars were analyzed and compared. Further, three-dimensional non-linear FEA models of modified push-out tests were established and validated by the test results. The shear mechanism of each component and the effects of rubber ring thickness on shear behaviors were discussed. Finally, based on the test results from this paper and literature, the yield load equations and shear capacity equations of PBLs and RPBLs were put forward.

Table 1
Parameters of specimens.

Specimen	d /mm	d_s /mm	t_r /mm
PB	60	20	–
RPB-1	60	20	2
RPB-2	60	20	4
RPB-3	60	20	6

Note: d and d_s are the diameters of holes and perforated rebars; t_r is the thickness of rubber rings.

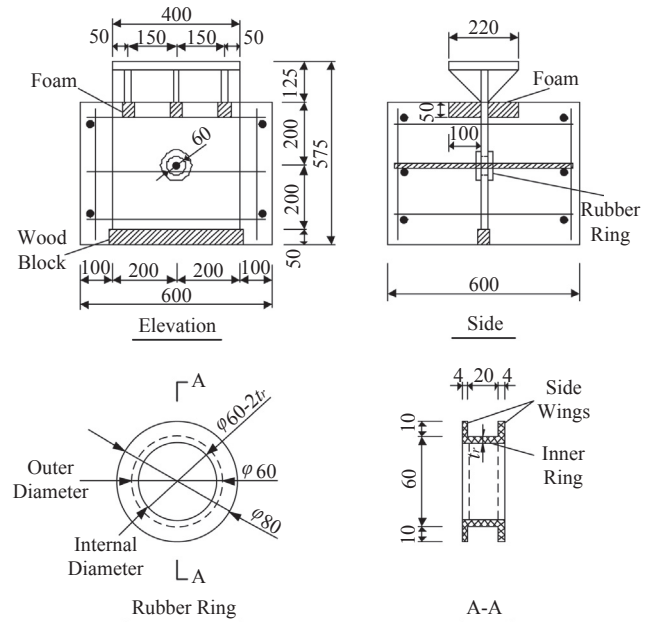


Fig. 3. Specimen configuration/mm.

2. Experimental program

2.1. Test specimens

To investigate the effect of rubber rings on the shear behavior of perfobond connectors, four modified push-out test specimens with rubber ring thickness of 0 mm, 2 mm, 4 mm and 6 mm were designed and fabricated. Table 1 and Fig. 3 shows the parameters and configuration of specimens, wherein the perfobond steel plate has a thickness of 20 mm. Triangle ribs were welded between the bearing plates and the perfobond steel plates to prevent buckling during the loading process. Plastic foams with 50 mm height were mounted below the ribs to avoid the contact between ribs and concrete blocks. Similarly, 50 mm high wood blocks were placed under the perfobond steel plates before casting to remove the end pressure. In previous experiments, some scholars used grease or pasting foam to remove the bond and friction between steel plates and concrete blocks [7–9,15]. However, they do exist and develop contributions to shear behaviors in practical applications, so that the specimens were not greased to reflect the real shear behavior of connectors.

The rubber ring consists of an inner ring and two side wings which can prevent rubber rings from falling off during concrete casting. As rubber rings have low hardness, the installation on site can be realized by manually compressing rubber rings into holes and restoring the geometry after inner rings contact with hole walls. Therefore, the practical applications of rubber rings are simple and efficient. The rubber rings with various thicknesses and the specimen assembly are shown in Fig. 2.

2.2. Material properties

Three groups of 150 × 150 × 150 mm cubic and 150 × 150 × 300 mm prismatic concrete samples with the nominal strength of 50 MPa (Grade C50) were fabricated during casting to evaluate concrete material properties. The test results show that the concrete has 52.1 MPa cube compressive strength f_{cu} , 43.0 MPa axial compressive strength f_c , 4.6 MPa cube splitting strength f_t and 40.6 GPa elastic modulus E_c . As regards the rubber material, the rubber rings employed in the test were made by natural rubber with the Shore hardness of 61 degrees. The tensile strength and the elongation at break of rubber samples are 20.7 MPa and 549%.

The nominal yield strength of steel plates, perforated rebars and distributed reinforcements are 345 MPa, 400 MPa and 335 MPa, respectively. The average yield strength and tensile strength of 9 rebars from the same batch are 479 MPa and 597.6 MPa. The yield strength of fractured perforated rebars after loading are 438.3, 413.8, 470.7 and 508.0 MPa, and the corresponding tensile strength are 562.3, 560.7, 581.6 and 617.9 MPa.

2.3. Test setup and instrumentation

Fig. 4 shows the test setup and instrumentation. Two short rebars were welded to both sides of steel plates and wrapped by plastic foams to obtain the slips at holes of perfobond connectors. The plastic foams were removed before specimen loading, which makes the space below short rebars no less than 50 mm. Two LVDTs with a precision of 1/1000 mm were positioned between concrete blocks and short rebars. Besides, a 2 mm thick lime cushion layer was placed on the top steel plate to avoid eccentric loading.

The specimens were loaded by a servo-hydraulic system with 20,000 kN loading capacity. The loading procedure included the force-controlled cyclic preloading steps and the displacement-controlled monotonic loading step. In the preloading steps, the load ranged from 5% to 40% of the estimated ultimate load. The loading speed was respectively 2 kN/s and 0.2 mm/min in the preloading and the formal loading steps. The total time spent on loading one specimen was more than 15 min.

Fig. 5 shows the strain gauge arrangement on steel plates and perforated rebars, which aims at revealing the shear mechanism of rubbering perfobond connectors. Five strain gauges parallel to the loading direction were arranged on a horizontal cross-section of steel plates which is 60 mm from the center of holes. Also, five strain gauges were mounted on each perforated rebar. Among the five gauges, three of

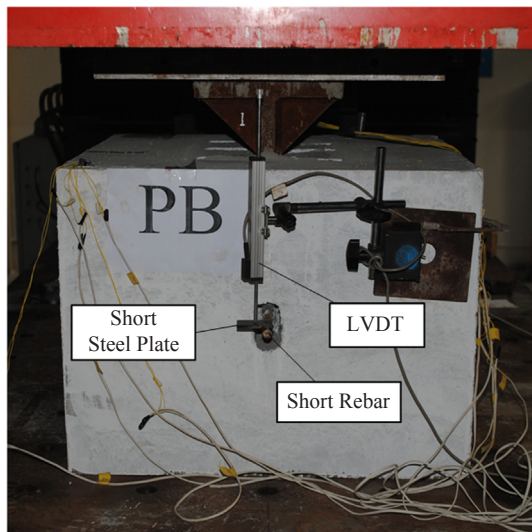


Fig. 4. Test setup and instrumentation.

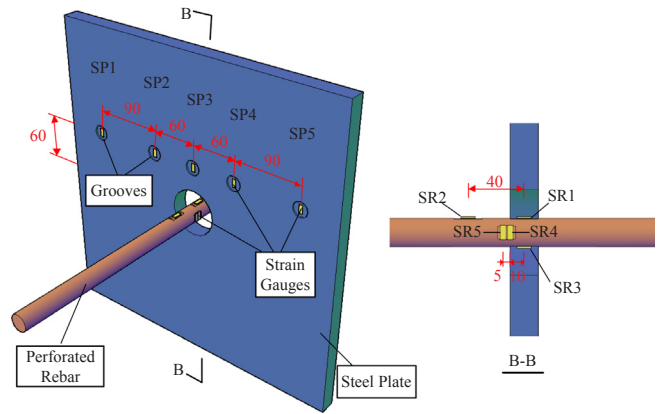


Fig. 5. Strain gauges on steel plates and perforated rebars/mm.

them on the upper or lower edges are parallel to rebar longitudinal direction, while the other two on the side are perpendicular to the longitudinal direction.

3. Test results

3.1. Load-slip curves

Table 2 summaries the test results, where the yield load V_y is defined as the peak load in the plastic stage after the cracking load V_c , and the corresponding slip is the yield slip s_y . Also, the shear stiffness k_s is defined as the ratio of yield load to yield slip. Moreover, the shear capacity V_u and ultimate slip s_u respectively represent the load and slip leading to the failure of the specimens. Compared with ordinary perfobond connectors, the yield slips of specimens with 2 mm, 4 mm and 6 mm thick rubber rings increase by 304%, 509% and 745%. Since rubber rings reduce the confinement effect of rebars and holes wall on concrete dowels, the yield loads of RPBLs are about 70% of those of PBLs. However, the reduction of ultimate shear capacity is around 15% due to the dominant contribution of perforated rebars to shear capacity. Fig. 6 shows the relationship between shear stiffness and rubber-ring thickness, indicating that setting rubber rings can effectively decrease the shear stiffness of perfobond connectors.

Fig. 7(a) presents the load-slip curves of specimens, where the slips represent mean values of the two LVDTs. The curve of specimen PB without rubber rings includes four stages. The initial stage is a linear stage with high stiffness, mainly relying on the bond between steel plates and concrete to resist the applied load. Then cracking occurred when the load increased to V_c , which marks the end of the first stage. Followed by the damage of bond, the loads are mainly undertaken by concrete dowels and perforated rebars. Further, the applied load reached the yield load V_y , which is accompanied by shear failures of concrete dowels. As the slip grew, the load dropped slightly resulting from the descending bond stress. Although there remained some residual bond forces and mechanical friction at shear planes of concrete dowels, the loads were mainly taken by the perforated rebars after the fracture planes formed. With the substantial increment of slip, the loads approximately linearly rose to the shear capacity V_u in the hardening stage until shear fracture planes of perforated rebars formed. Finally,

Table 2 Test results.

Specimen	V_c /kN	V_y /kN	s_y /mm	k_s /(kN/mm)	V_u /kN	s_u /mm
PB	401.2	491.7	1.12	439.0	555.2	20.69
RPB-1	394.4	361.0	4.52	79.9	447.8	28.10
RPB-2	392.0	339.7	6.82	49.8	489.4	36.79
RPB-3	421.2	316.0	9.46	33.4	472.6	36.66

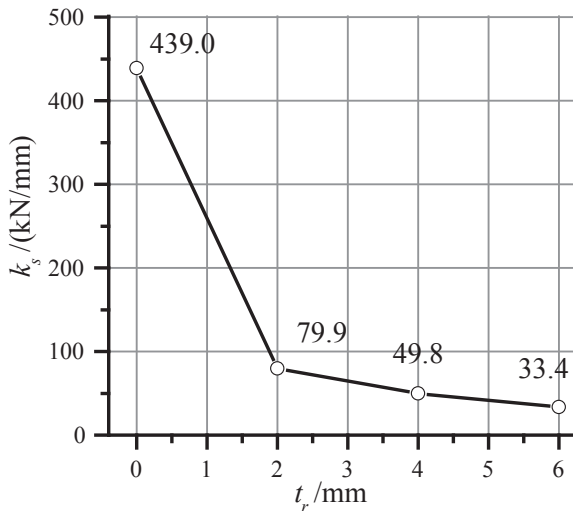


Fig. 6. Relationship between shear stiffness and rubber-ring thickness.

perforated rebars were sheared off followed by the sharp load drops in the curves.

Compared with specimen PB, fewer loads were carried by concrete dowels and perforated rebars in the first stage in rubber-ring perfobond connectors. It is noted that the cracking loads of four specimens are close indicating that the applied loads in the initial stage are mainly undertaken by the bond. Subsequently, the load dropped dramatically after the bond damaged. As the rubber thickness increases, the yield load V_y and the yield slip s_y respectively reduce and grow. The reason is that the rubber rings with little stiffness postpone the shear resistance of perfobond connectors, and also decrease confinement effects on concrete dowels. In the hardening stage, the ultimate slip s_u increases with the thickness of rubber rings. However, the increment is limited by the deformation capacity of perforated rebars.

3.2. Failure modes

Fig. 8 shows the crack distributions of concrete blocks. On the top surface and the two side surfaces perpendicular to the perfobond steel plates the cracking occurred, while no cracks were found on the side surfaces parallel to the steel plates. The top surface cracks start from the edges of steel plates, and the side surface cracks are always in a vertical direction. In other words, the cracking is along the edges of steel plates and mainly caused by the damage of bond.

The concrete blocks were cut off after loading to present the shear fracture planes, as shown in Fig. 9. As the slips increased, the upper part

of concrete dowels was compacted, and the rubber rings close to the loading side were utterly squashed. Both of the side wings encountered large deformation and were sheared off. The shear planes of PBLs are parallel to steel plates, while the shear planes of rubber-ring perfobond connectors incline with steel plates. The reason is that rubber rings enlarge the span of concrete dowels, leading to a bending force mode and tensile cracking at the lower part of concrete dowels. Besides, there are slip traces on steel plates and concrete shear planes, indicating the existence of friction in the sliding process.

The ultimate failure modes of specimens are the fractures of perforated rebars. With or without rubber rings, the failure modes are the tension-shear fracture planes with necking, as shown in Fig. 10(a). Perforated rebars may have two fracture planes at positions of steel plate surfaces. However, sometimes only one fracture plane forms accompanied by large tensile-shear deformation on the other side. Fig. 10(b) shows the rebar shape inside concrete blocks, indicating the bending deformation is small compared with the shear deformation near steel plates.

3.3. Strains on steel plates

Fig. 11 shows the steel plate strains in PB and PRB-3 at early loading stages. The vertical compressive strains linearly increase with the applied load. Due to the damage of strain gauges, the stages after cracking are omitted in the figures. The strains of the gauges equidistant from the perforated rebars are expected to be similar. The differences in strain values might be caused by the unevenness of the loading. Overall, the average strains of SP2 and SP4 are relatively large, followed by the average strains at the SP1 and SP5. The minimal strains occur at SP3 locating at the middle of perfobond plates. Given that SP2 (SP4) and SP1 (SP5) are respectively 60 mm and 150 mm from the central line, the vertical strains around the holes transferring to holes by the path with about 45 degrees to the vertical direction, which is consistent with the numerical results in the next section. Also, the strain values at the edge of perfobond plates are smaller than those at the core load-transfer region around holes. The strains of SP3 are minimal and not enlarged by the contact forces between concrete dowels and hole walls, which demonstrates that at early loading stages strains on the perfobond plates are caused by the bond stress, and the shear forces are mainly undertaken by the bond forces.

3.4. Strains on perforated rebars

Fig. 12 shows the load-strain relationships of perforated rebars. Since the shear force is mainly resisted by bond at the early loading stage, perforated rebars have small strains. However, the strains rise rapidly with the increase of slip after cracking load. The tensile strain of

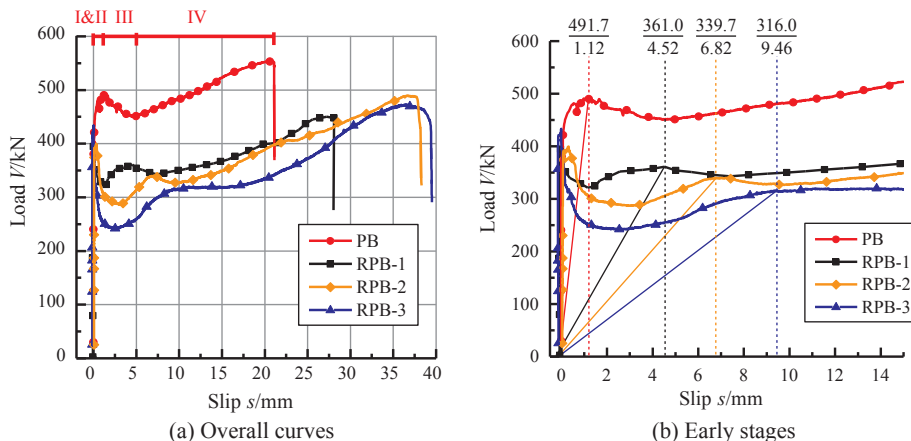


Fig. 7. Load - slip curves.

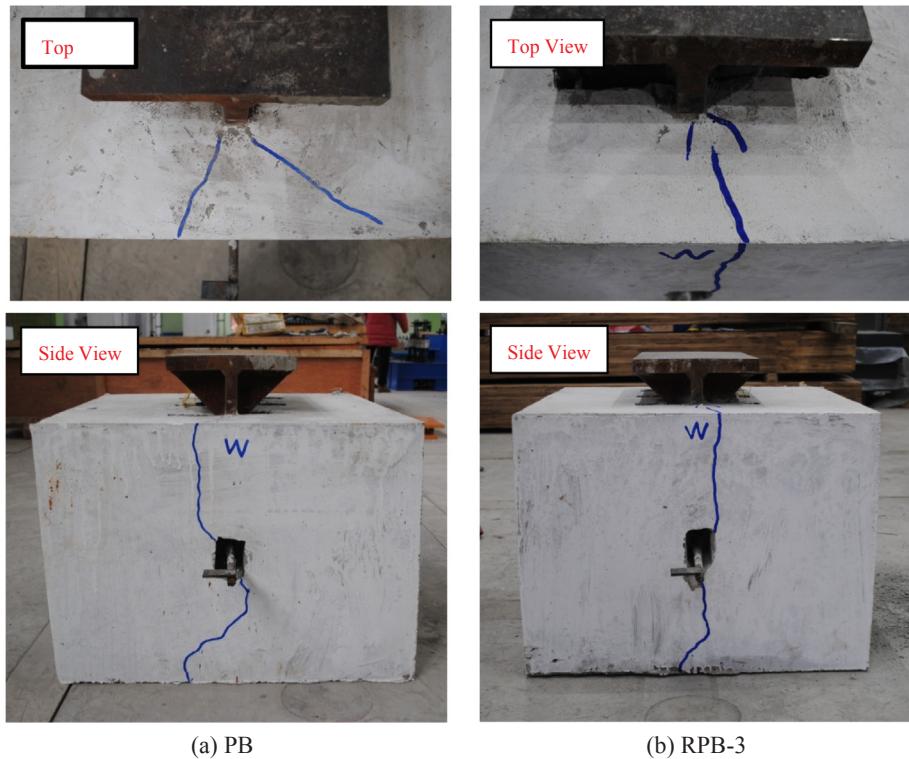


Fig. 8. Crack distributions on concrete blocks.

SR3 increases fastest among the five strain gauges, followed by the compressive strain of SR1 and the tensile strain of SR2, which reflects the bending characteristics of perforated rebars. As the slip increases further, the strains of SR4 and SR5 rose. SR4 is in compression while SR5 is in tension, indicating that the shear planes in PB are 10 mm to 15 mm from the center of circle holes. Note that SR5 changed from compressive strain to tensile strain. The reason is that the location of the shear plane moved as the slip and deformation developed. However, both SR4 and SR5 are in compression in RPB-3, indicating that shear planes of perfobond connectors with rubber rings are farther from the centerline. As mentioned before, rubber rings enlarge the span diameter ratio of concrete dowels and perforated rebars.

4. Finite element analysis

4.1. Finite element model

3-D nonlinear finite element models of modified push-out tests are established by ABAQUS/Explicit to investigate the shear behavior of rubber-ring perfobond connectors. The models consist of perfobond

steel plates, concrete blocks, rubber rings, perforated rebars, distribution reinforcements and the ground, as shown in Fig. 13. The distribution reinforcements are simulated by the linear truss element T3D2, and the ground is set as a rigid surface. All the rest parts are built by the 3-D 8-node reduced integration element C3D8R. As for the boundary conditions, the ground reference point is fixed in the model. Contact interactions are built between the rigid ground and the bottom surface of concrete blocks, as well as at the interfaces between different components. Since the longitudinal slips of perforated rebars observed in the tests are negligible, tie constraints are set at the interfaces between perforated rebars and concrete blocks. Also, nonlinear material constitutive laws and bond forces are considered in the models.

4.2. Material modeling

4.2.1. Constitution of concrete

The concrete properties are simulated by Concrete Damage Plasticity Model (CDPM) provided by ABAQUS [23]. The yield criterion used in this model was proposed by Lubliner et al. [24] based on the Drucker-Prager model and improved by Lee and Fenves [25]. The equations are as follows:

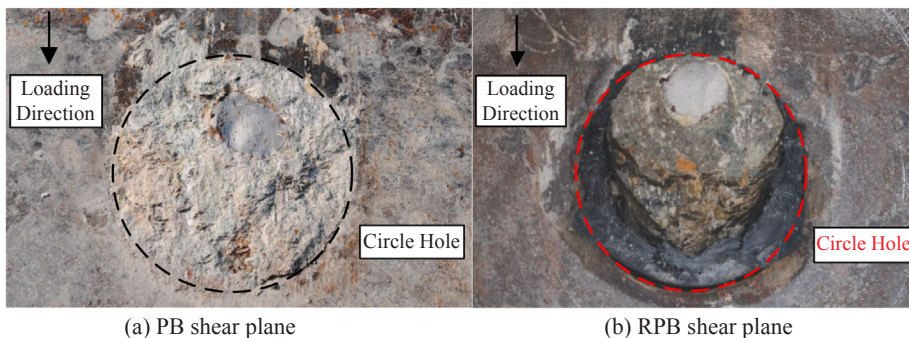
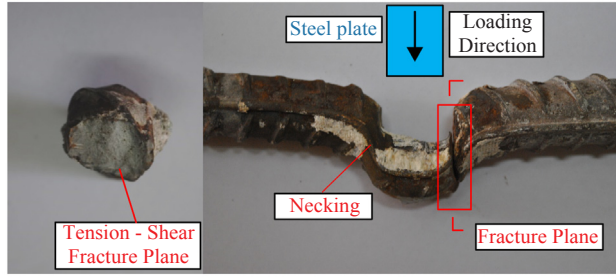
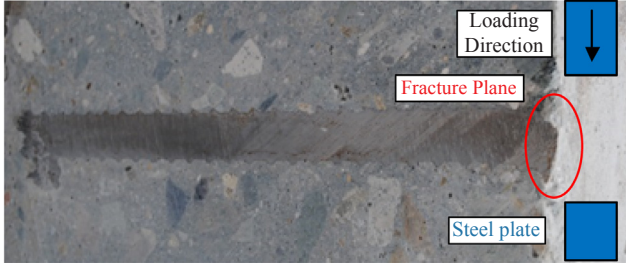


Fig. 9. Shear planes of perfobond connectors.



(a) Rebar fracture planes



(b) Rebar shape inside concrete block

Fig. 10. Failure modes of perforated rebars.

$$F = \frac{1}{1 - \alpha} (\sqrt{3J_2} - \alpha I_1 + \beta \langle \sigma_{\max} \rangle - \gamma \langle -\sigma_{\max} \rangle) - \sigma_{cn} (\tilde{\epsilon}_c^{pl}) = 0 \quad (1)$$

$$\alpha = \frac{(\sigma_{b0}/\sigma_{c0}) - 1}{2(\sigma_{b0}/\sigma_{c0}) - 1} \quad (2)$$

$$\beta = \frac{\sigma_{cn} (\tilde{\epsilon}_c^{pl})}{\sigma_m (\tilde{\epsilon}_t^{pl})} (1 - \alpha) - (1 + \alpha) \quad (3)$$

$$\gamma = \frac{3(1 - K_c)}{2K_c - 1} \quad (4)$$

where the Macauley bracket $\langle * \rangle$ is defined as $\langle x \rangle = (|x| + x)/2$; I_1 and J_2 are the first stress invariant and the second deviator stress invariant; σ_{\max} is the maximum principal stress; σ_{b0}/σ_{c0} is the ratio of initial equibiaxial compressive yield stress to initial uniaxial compressive yield stress with the default value of 1.16; σ_{cn} and σ_m are the uniaxial compressive and tensile stresses of unconfined concrete; $\tilde{\epsilon}_c^{pl}$ and $\tilde{\epsilon}_t^{pl}$ are the compressive and tensile equivalent plastic strains, respectively.

The parameter K_c is the ratio of the second stress invariant on the tensile meridian to that on the compressive meridian. When $K_c = 1$, the yield surface in the deviation plane is circular, which is consistent with the classical Drucker-Prager model; when $K_c = 0.67$, that is a triaxially

symmetrical convex smooth triangle, similar to the William-Warnke model. The value of K_c increases with the growth of the hydrostatic pressure [26–28]. Since the Drucker-Prager criterion is suitable for materials which expand when sheared, and more in line with the stress state of concrete dowels near shear planes, K_c is determined as 0.9 after numerical tests. The expansion angle is taken as 30 degrees [6]. The other parameters are determined by the recommended values in the ABAQUS User's Manual [23]. The flow potential eccentricity and viscosity coefficient are 0.1 and 0.

Fig. 14(a) shows the compressive stress-strain curve provided by the CEB-FIP MC2010 [29]. The ascending segment can be calculated by Eq. (5) and (6), where ϵ_c and σ_c are the strain and stress at any point on the curve; ϵ_{cp} is the strain corresponding to the peak compressive stress, $\epsilon_{cp} = 0.0025$. The descending segment is assumed to be linear and end at 85% of the compressive strength [30]. The ultimate strain is taken as 0.0033 according to [29]. As for tensile behavior, the axial tensile strength f_t is calculated by the splitting tensile strength and Eq. (7) provided by CEB-FIP MC 1990 [31]. The initial stage is assumed as a straight line with the slope of Young's modulus. The tensile behavior after cracking is defined by the stress-crack width relationship referred to Hordijk et al. [32], as shown in Fig. 14(b) and Eq. (8).

$$\frac{\sigma_c}{f_c} = \frac{k \cdot \eta - \eta^2}{1 + (k - 2) \cdot \eta} \quad (5)$$

$$k = E_c \cdot \epsilon_{cp} / f_c, \quad \eta = \epsilon_c / \epsilon_{cp} \quad (6)$$

$$f_t = 0.9 f_{t,s} \quad (7)$$

$$\frac{\sigma_t}{f_t} = \left[1 + \left(c_1 \frac{w}{w_c} \right)^3 \right] \cdot \exp \left(-c_2 \frac{w}{w_c} \right) - \frac{w}{w_c} (1 + c_1^3) \cdot \exp(-c_2) \quad (8)$$

where w and σ_t are the crack width and the tensile stress at any point of the curve; w_c is the crack width at the tensile stress of 0, $w_c = 5.14 G_F / f_t$ (mm); G_F is the fracture energy required to create a unit area of stress-free crack [33], $G_F = 0.073 f_c^{0.18}$ (N/mm); The coefficient c_1 and c_2 are taken as 3 and 6.93, respectively [6].

4.2.2. Constitution of steel and rubber

The ideal elastic-plastic trilinear model considering hardening is employed to simulate steel plates and rebars [6], as shown in Fig. 14(c). The strain range of the horizontal yielding branch is from 1 to 10 times the elastic strain ϵ_y . The ultimate strain ϵ_u is assumed as 0.2. In this study, steel plates and distributed reinforcements used the nominal strengths, while perforated rebars employed the measured strength.

Rubber is regarded as an isotropic and incompressible hyperelastic material whose material constitution can be described by strain potential energy U . Without isometric biaxial and planar tests, only uniaxial tensile tests of rubber specimens were conducted in this paper.

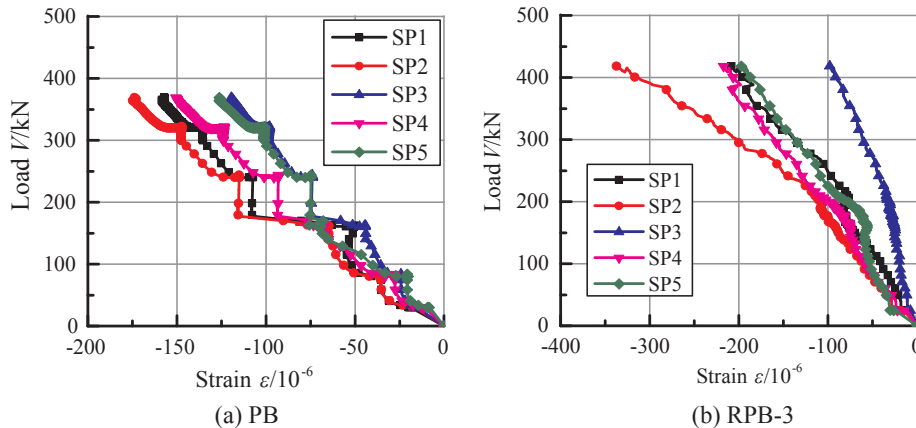


Fig. 11. Load – strain relationship on steel plates.

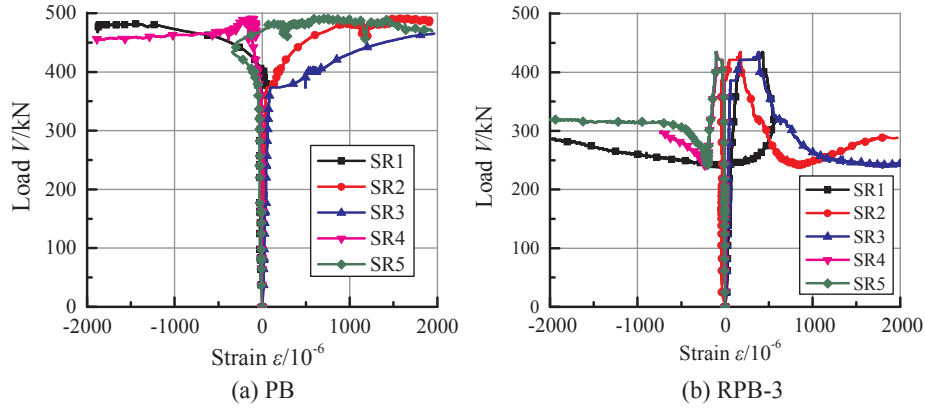


Fig. 12. Load – strain relationship on perforated rebars.

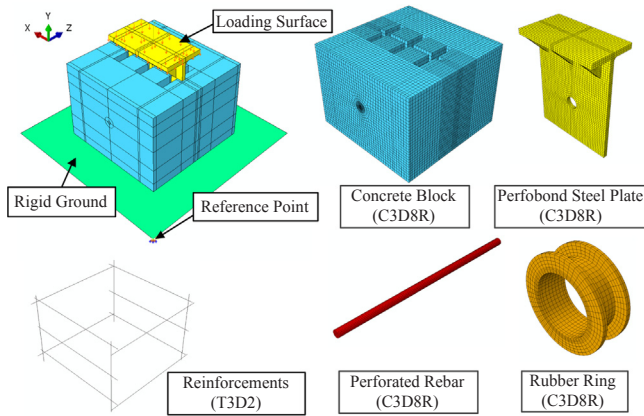


Fig. 13. FEA model of modified push-out tests.

Among the several strain potential models provided by ABAQUS, it is recommended to select a reduced polynomial by using limited experimental data for calibration [23]. The equation is as follows:

$$U = \sum_{i=1}^N C_{i0} (\bar{I}_1 - 3)^i + \sum_{i=1}^N \frac{1}{D_i} (J_{el} - 1)^{2i} \quad (9)$$

Fig. 14(d) shows the fitting curve based on the test data, where the material coefficients for controlling shear behavior and volume compression $C_{10} = 0.587$ MPa, $C_{20} = 0.0143$ MPa, $D_1 = 0.0866$ MPa⁻¹ and $D_2 = 0$. However, since the rubber rings in perfbond connectors are confined by steel plates and surrounding concrete, 50 times of the strain potential energy are used in the modeling after trial calculation, i.e., $C'_{10} = 29.4$ MPa, $C'_{20} = 0.72$ MPa, $D'_1 = 0.0017$ MPa⁻¹ and $D'_2 = 0$.

4.3. Contact properties

In addition to establishing constraints (Tie) between perforated rebars and concrete blocks, contact pairs are built between the rigid ground and the bottom surfaces of concrete blocks, steel plate surfaces and concrete blocks, circle holes and concrete dowels, rubber rings and steel plates as well as concrete components. The normal behavior about pressure-overclosure is set as “hard”, which means the interfaces cannot be penetrated but are able to separate. By considering the concrete blocks were directly set on the loading table in the experiments, the friction coefficient between the loading table and bottom surfaces of specimens is assumed as 0.3 after test calculations.

Since the cohesive layers have negligible thicknesses and fail at relatively large slips, the surface-based cohesive behavior is employed to simulate the bond between steel and concrete. The normal and tangential cohesive behaviors are considered as uncoupled. The

maximum separation/slip failure criterion is used in the models. As shown in Fig. 14(e), before damage occurs the cohesive stress has a linear relationship with the separation/slip, where τ_i is the cohesive strength and δ_i^0 is the maximum undamaged normal separation or tangential slip, which equals to 0.61 mm according to the test results from He et al. [14]. Further, the bond stress decreases by the exponential evolution rule [23] with the rate of 1. δ_f^i represent the effective separation/slip at fully failure state and is taken as 5.5 mm by numerical tests.

4.4. Model validation and shear mechanism analysis

4.4.1. Load-slip curves

Fig. 15 shows the test and FEA load-slip curves. Overall, the simulated curves agree well with the test results. The FEA models can reflect the whole failure process of PBLs and RPBLs, including the damage of bond, the yielding of concrete dowels and perforated rebars, and the fractures of perforated rebars. Also, the good predictions of cracking loads, yield loads and shear capacities are realized in the simulation. The stiffness of the FEA models are less than the counterpart test models. The probable reason is that the bond stiffness was underestimated in the models. The test results in [14] reflected the global stiffness of the bond, which may be different from the local cohesive behavior. The lower accuracy of RPBL models may result from the rubber properties. Although the uniaxial tensile tests were conducted on rubber samples, the rubber properties under constraint were not obtained from tests. Additional works are underway to obtain more reasonable bond behavior and rubber properties. Note that the slopes in the rebar hardening stage and the ultimate slips are respectively larger and smaller than those in tests. The reason is that the rebar property is simulated by the stress–strain curve, which should be improved in the upcoming works.

4.4.2. Strain distribution of steel plate

Fig. 16(a) compares the steel plate strains in RPB-2 with that in FEA models. Numerical results show similar tendencies as test results that the steel plate strains linearly increase with the load before bond damage occurs. Also, the strains at SP2 are in turn larger than those at SP1 and SP3. As shown in Fig. 16(b), under the cracking load the vertical strains above holes are relatively small, indicating concrete dowels and perforated rebars are less stressed, which further demonstrates that the shear forces are mainly undertaken by bond forces at the early loading stage. The maximum vertical strains appear on the sides of holes, accompanying with relatively large strains in the band-shaped region inclined about 45 degrees.

4.4.3. Shear mechanism of concrete dowels and rubber rings

Fig. 17 shows the plastic principle compressive strains in the

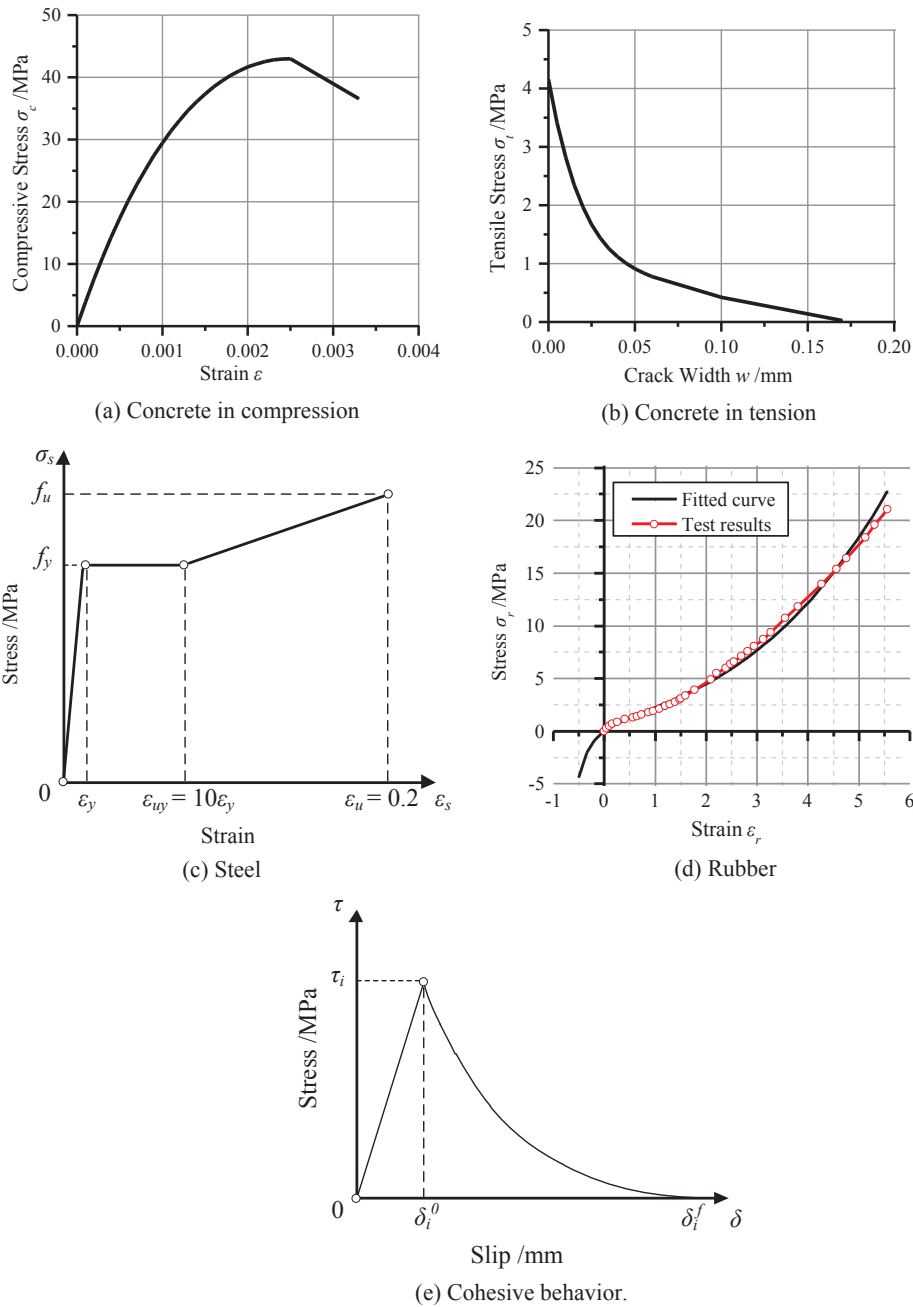


Fig. 14. Material constitution.

concrete dowels under the yield load. The maximum principle compressive strains appear in the upper part of concrete dowels between the steel plates and perforated rebars, where the concrete is confined by steel plates, perforated rebars and surrounding concrete. Compared with the ordinary perfbond connector, the confinement of surrounding concrete is diminished by employing rubber rings, so that the strains in the RPB models are more significant than those in the PB model. Also, the area with strain concentration decreases with the increase of rubber ring thickness, resulting in a reduction of yield loads. It is clear that the shear planes form in the concrete dowels under the yield load. The shear planes in the PB model are perpendicular to the perforated rebar, while those start from the steel plates to the edges of side wings of rubber rings in the RPB models. It indicates that the thicknesses of inner rings and side wings can affect the positions of shear planes.

Fig. 18 shows the Mises stress and deformation of the rubber rings under the cracking load and the yield load. Apparently, before the

damage of bond forces the stress in rubber rings is relatively small as well the deformation is negligible. The Mises stress and deformation of rubber rings rise significantly when the loads approach the yield load. The stress concentrates in the region contacting with the upper of hole walls and increases with the thickness of rubber rings. In the rubber rings with thicknesses of 4 mm and 6 mm, the local maximum Mises stresses are 226 MPa and 230 MPa, respectively. With respect to the deformation, the regions contacting with the hole wall are squashed, and the inclined shear planes form near the upper of side wings, which is consistent with the failure mode in Fig. 9.

4.4.4. Shear mechanism of perforated rebars

Fig. 19 shows the Mises stress and deformation of perforated rebars at the ultimate shear capacity of models. There are two tensile-shear fracture planes formed on both sides of steel plates. It is noted that the Mises stresses at tensile-shear fracture planes reach the tensile strength

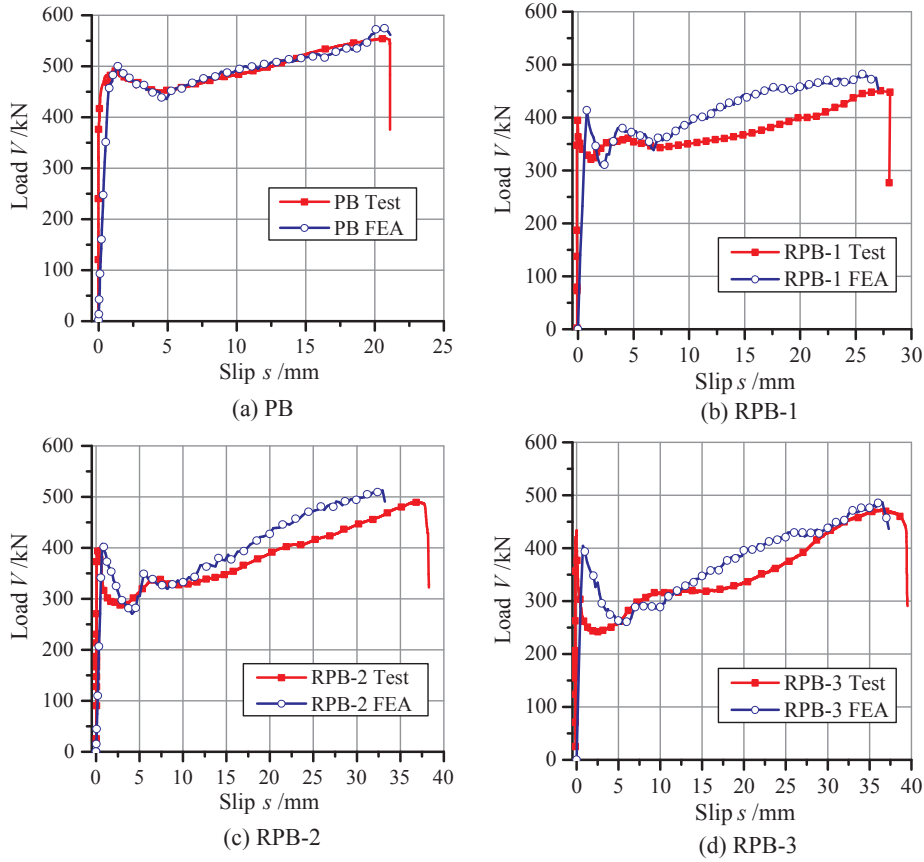


Fig. 15. Comparison of load - slip curves.

of rebars, so does the middle segment with a length of steel plate thickness. When the loaded models approach failure stage, apparent shear deformation can be seen at fracture planes, which is consistent with the cut surface shown in Fig. 10(a). Also, the failure shear deformation from PB to RPB-3 increases with the growth of ultimate slip.

4.4.5. Parametric study

Furthermore, 11 models with various rubber thicknesses were carried out by the validated model to investigate the effects of rubber ring thickness on the shear behavior. In the parametric analysis process, the geometry of components and the material properties are consistent with those employed in the validated models. The bond actions are eliminated in the models. Table 3 shows the parameters and results of the parametric study, which are analyzed in the next section.

5. Shear capacity equations

5.1. Existing equations

Eq. (13)–(17) as shown below are the existing shear capacity equations of perfbond connectors based on modified push-out test results. Where A_c is the area of concrete dowels; A_s and A_t are the area of perforated rebars and transverse reinforcements; f_y' is the yield strength of transverse reinforcements; τ_b and A_b are the bond strength and contact area between steel plates and concrete blocks; t is the thickness of perfbond steel plate, and n is the number of holes.

Zhang et al. [12] proposed Eq. (10) by the regression analysis on 31 specimens test results. They consider that the shear capacity is mainly provided by concrete dowels and perforated rebars. Tensile strength is

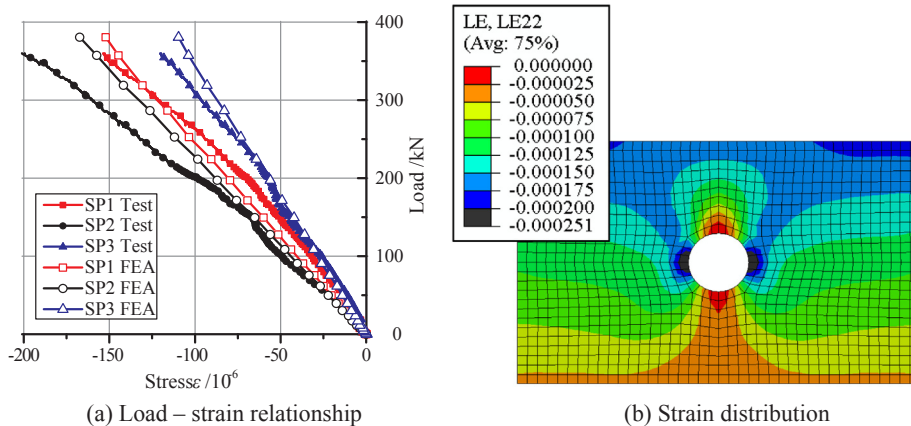


Fig. 16. Comparison of strains on steel plates.

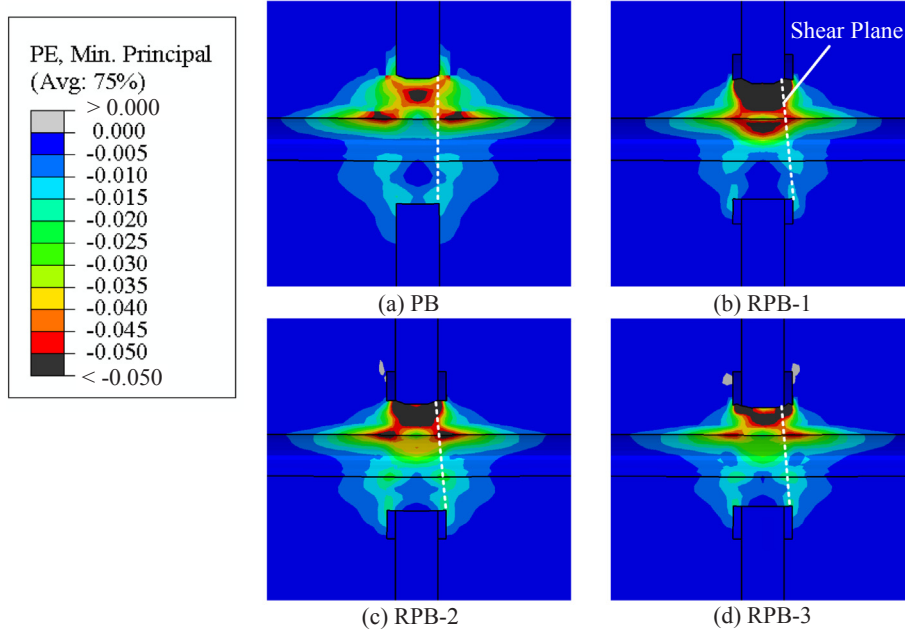


Fig. 17. Plastic principle compressive strains in concrete dowels.

chosen to calculate the contributions of perforated rebars in their equation. Wang et al. [9] carried out the modified push-out tests including 33 specimens by horizontal loading and presented Eq. (11) where the coefficient α , β and δ are 0.9974, 0.1293 and 220 kN. They suppose that transverse reinforcements make contributions to the shear bearing capacity, while the contributions of concrete dowels are negligible. The bond between steel plates and concrete is taken into account by the constant term δ in the equation. Based on 24 groups modified push-out test results, Wang et al. [13] proposed Eq. (12), in which the shear capacity is affected by concrete dowels, perforated rebars and transverse reinforcements. Yield strength is employed to consider the contributions of perforated rebars and transverse

reinforcements.

$$V_u = 0.95 \times (2A_c f_c) + 0.94 \times (2A_s f_u) \tag{10}$$

$$V_u = \alpha(2A_s f_u) + \beta(2A_{tr} f'_y) + \delta \tag{11}$$

$$V_u = 0.498A_c \sqrt{f_c} + 0.255A_s f_y + 0.065A_{tr} f'_y \tag{12}$$

He et al. [14] conducted modified push-out tests with 12 specimens to analyze the independent contributions of concrete dowels, perforated rebars and bond forces and put forward Eq. (13). Zhao et al. [18] investigated the influence of hole diameter, perforated rebar diameter, bond, concrete strength and transverse reinforcements on shear bearing

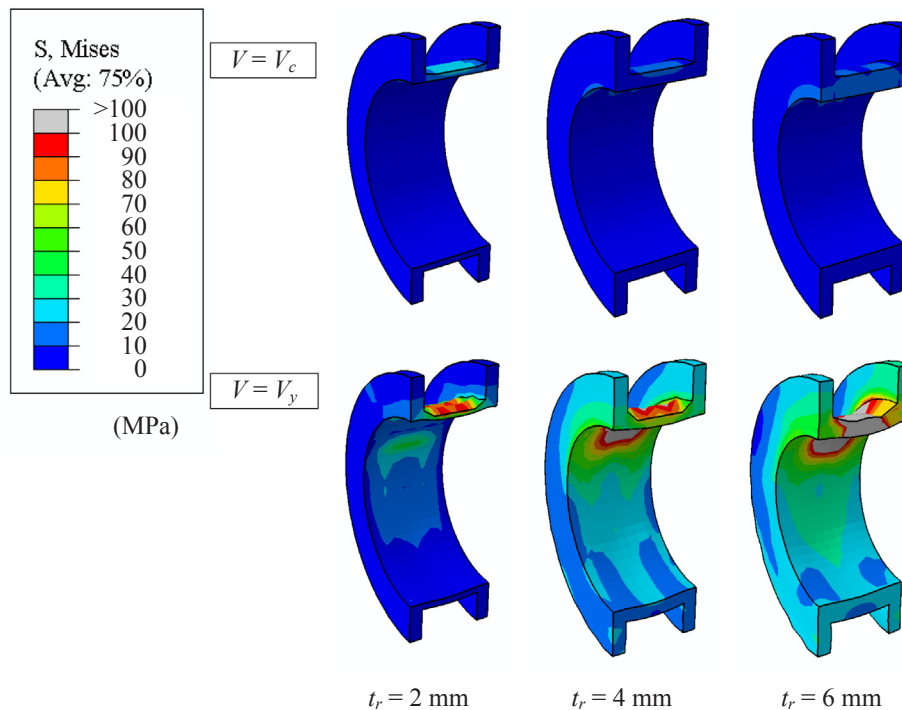


Fig. 18. Mises stress in rubber rings.

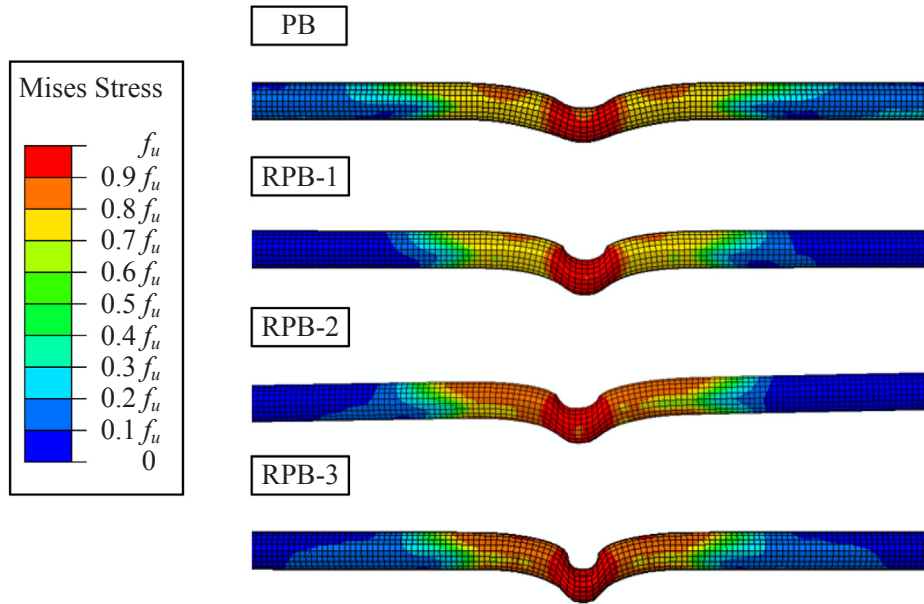


Fig. 19. Mises stress and deformation of perforated rebars.

capacity by 18 modified push-out specimens with two holes. They explained the contributions of transverse reinforcements to shear capacity by the expansion – clamping force model and put forward Eq. (14).

$$\begin{cases} V_u = \tau_b A_b + 1.06 A_c f_{cu} + 2.09 A_s f_y \\ \tau_b = -0.022 f_{cu} + 0.306 \sqrt{f_{cu}} - 0.573 \end{cases} \quad (13)$$

$$V_u = 0.65 (A_{tr} f'_y + A_s f_y) + (5.512 d^2 - 0.0028 d^4) n \sqrt{f_c f_y} \quad (14)$$

Table 4 compares the test results with the calculated results by the existing equations. Although ignoring the effects of bond and transverse reinforcements, Eq. (10) has minimal errors among the existing equations. The reasons might be that the contributions of concrete dowels are overestimated, and tensile strength is taken to calculate the shear resistance of perforated rebars. Eqs. (11) and (12) use different strengths to estimate the contributions of perforated rebars, as well the coefficient difference is also substantial. The contributions of transverse reinforcements are taken into account in both equations. However, they both predict larger shear bearing capacity than tests.

Eq. (13) takes account of the contributions of bond forces to shear bearing capacity, while ignores the effect of transverse reinforcements. The calculation errors for specimens without and with rubber rings are 6% and around 20%, respectively. In Eq. (14) concrete dowels are considered irrelevant to the shear bearing capacity. The contributions of perforated rebars are analyzed through a beam model supported by a semi-infinite elastic foundation. The overall errors of Eq. (14) are relatively small. However, the calculated results for specimens with and

Table 4

Calculated results by existent equations/kN.

Specimen	Eq. (10)	Eq. (11)	Eq. (12)	Eq. (13)	Eq. (14)	Test
PB	537.4	642.1	616.6	588.3	505.7	555.2
Error/%	-3.2	15.6	11.1	6.0	-8.9	
RPB-1	506.7	641.1	583.9	549.9	493.8	447.8
Error/%	13.2	43.2	30.4	22.8	10.3	
RPB-2	491.3	654.2	617.3	568.5	521.0	489.4
Error/%	0.4	33.7	26.1	16.2	6.5	
RPB-3	487.1	676.9	635.8	575.7	538.4	472.6
Error/%	3.1	43.2	34.5	21.8	13.9	

without rubber rings are about 10% larger and smaller than the experimental results. The possible reason is that the term with respect to concrete dowels should be added for PBLs, as well the expansion – clamping action of transverse reinforcements is overestimated.

5.2. Yield load equations

The equations above are used to calculate the shear capacity of PBLs in the ultimate bearing state, where the corresponding slip usually exceeds 10 mm. On the contrary, the yield load is the local peak load on shear-slip curves, which reflects the shear performance of perfbond connectors at the serviceability state. The corresponding slip at the yield load is usually between 1 mm and 5 mm.

Eq. (15) is the shear capacity equation for a single hole of PBLs proposed by Zheng et al. [6] based on 21 push-out test results and 87

Table 3

Parametric study results.

Model	t_r /mm	A_c /mm ²	V_y /kN	V_u /kN	V_c /kN	V_{Eq} /kN	$V_y V_s$ /kN	β
F-RPB-tr0	0	2826	414.6	569.4	166.8	404.5	177.0	1.00
F-RPB-tr0.5	0.5	2733	397.7	494.8	160.6	398.3	160.1	0.94
F-RPB-tr1	1	2641	384.9	519.2	154.5	392.2	147.3	0.90
F-RPB-tr1.5	1.5	2550	373.9	505.4	148.5	386.2	136.3	0.86
F-RPB-tr2	2	2462	362.2	509.3	142.6	380.3	124.6	0.82
F-RPB-tr3	3	2289	334.9	511.3	131.2	368.8	97.3	0.70
F-RPB-tr4	4	2123	314.9	517.2	120.1	357.8	77.3	0.61
F-RPB-tr5	5	1963	295.8	491.2	109.5	347.1	58.2	0.50
F-RPB-tr6	6	1809	275.2	475.1	99.3	336.9	37.6	0.36
F-RPB-tr8	8	1520	264.4	465.3	80.1	317.7	26.8	0.32

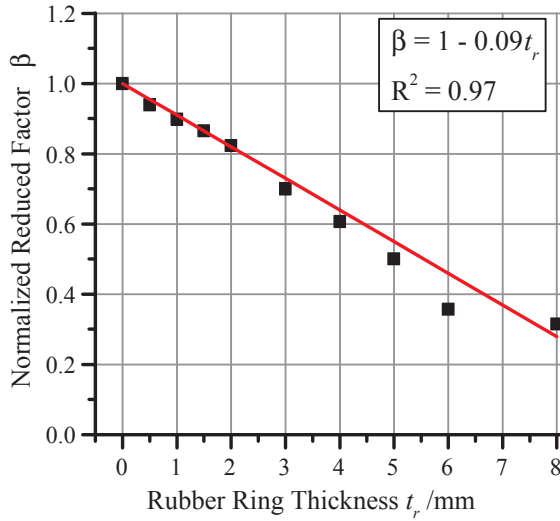


Fig. 20. Linear fitting of reduced factor β .

nonlinear FEA results, where A_h is the area of circle holes. The constraint effect of perforated rebars on concrete dowels is taken into account by the effective shear area ratio α_A , which equals 1 for the cases without perforated rebars, while the contributions of bond and transverse reinforcements are ignored. The peak slip corresponding to the shear bearing capacity is less than 5 mm.

$$\begin{cases} V_u = V_c + V_s = 1.76\alpha_A A_c f_c + 1.58A_s f_y \\ \alpha_A = 3.80(A_s/A_h)^{2/3} \end{cases} \quad (15)$$

In Table 3, V_{Eq} is the calculated result of Eq. (15); V_c and V_s are the calculated shear contribution by concrete dowels and perforated rebars from Eq. (15); β is the reduction factor defined as the ratio of $(V_y - V_s)$ to V_c normalized by the result of model F-RPB-tr0. It is noted that the yield load reduction with the growth of rubber ring thickness is more critical than that from Eq. (15). Therefore a strength reduction factor needs to be considered to improve the yield load equation. Fig. 20 shows the linear relationship between the rubber ring thickness t_r and the normalized reduction factor β . This indicates that the linear regression equation with high determination coefficient is efficient and feasible to reckon the influence of rubber ring thickness on the yield load.

Since the slip corresponding to yield load is relatively small, the expansion-clamping effects of the transverse reinforcements are ignored at this stage, but the influence of bond forces on yield loads should be

Table 6

Comparison between test and calculated results.

No.	Specimen	V_y /kN			V_u /kN		
		V_y test	Eqs.(16) and (17)	Error/%	V_u test	Eqs.(18) and (19)	Error/%
1	PB	491.7	522.9	6.3	555.2	579.2	4.3
2	RPB-1	361.0	322.4	-10.7	447.8	453.2	1.2
3	RPB-2	339.7	310.5	-8.6	489.4	463.6	-5.3
4	RPB-3	316.0	297.7	-5.8	472.6	481.6	1.9
5	C-b1r0d0	302.0	-	-	146.9	158.5	7.9
6	C-b0r0d1	247.0	229.3	-7.2	171.5	172.0	0.3
7	C-b1r0d1	370.0	337.3	-8.8	300.2	330.4	10.1
8	C-b1r1d0	300.5	300.5	0.0	326.0	-	-
9	C-b0r1d1	386.1	371.5	-3.8	449.0	406.6	-9.4
10	C-b1r1d1	461.1	479.5	4.0	547.0	565.1	3.3
11	S45-P10-C65u	492.4	493.2	0.2	493.0	522.3	5.9
12	S60-P10-C40	801.4	821.4	2.5	1033.5	970.8	-6.1
13	S60-P10-C55	977.5	912.7	-6.6	1130.0	1039.3	-8.0
14	S60-P10-C65	955.6	964.9	1.0	1101	1078.5	-2.0
15	S60-P8-C65	1055.8	969.2	-8.2	1087.5	993.6	-8.6
16	S80-P10-C65	1443.6	1472.2	2.0	1527	1592.9	4.3

taken into account. The contributions of the bond between steel plates and concrete to the yield load are introduced according to Eq. (13). When the concrete cube strength is between 30 and 70 MPa, the bond strength is in the range from 0.44 to 0.49 MPa. To simplify the equation, τ_b is assumed to equal to 0.45 MPa as a constant. Since rubber rings significantly increase the yield slip, the effect of bond on the yield load is ignored in RPBLs. Also, rubber rings decrease the confinement effects of hole walls on concrete dowels, so that the reduction factor β mentioned above should be considered. Based on the analysis above, Eq. (16) and (17) are put forward to calculate the yield load of PBLs and RPBLs.

$$V_y = n(1.76\alpha_A A_c f_c + 1.58A_s f_y) + 0.45A_b \quad (16)$$

$$\begin{cases} V_{y, rub} = n(1.76\alpha_A \beta A_c f_c + 1.58A_s f_y) \\ \beta = 1 - 0.09t_r, \quad t_r \leq 8 \text{ mm} \end{cases} \quad (17)$$

Table 5 summaries the parameters and results of modified push-out tests collected from this paper, He et al. [14] and Zhao et al. [18], where the yield load meets the definition in this paper. Table 6 and Fig. 21(a) compare the test results with the calculated results by Eqs. (16) and (17). The mean errors per each test program are -4.7%, -3.2% and -1.5%, respectively. The mean and maximum errors for all of the data are -2.9% and -10.7%, and the determination coefficient

Table 5

Summary of collected test data.

No.	Author	Specimen	d	n	d_s	f_c	f_y	f_u	A_b	A_{tr}	V_y	V_u
			/mm		/mm	/MPa	/MPa	/MPa	/cm ²	/cm ²	/kN	/kN
1	This paper	PB	60	1	20	43.0	438.3	562.3	3080	804	491.7	555.2
2		RPB-1	60	1	20	43.0	413.8	560.7	3080	804	361.0	447.8
3		RPB-2	60	1	20	43.0	470.7	581.6	3080	804	339.7	489.4
4		RPB-3	60	1	20	43.0	508	617.9	3080	804	316.0	472.6
5	He [14]	C-b1r0d0	60	1	0	46.1	388	549	2400	628	302.0	146.9
6		C-b0r0d1	60	1	0	46.1	388	549	2400	628	247.0	171.5
7		C-b1r0d1	60	1	0	46.1	388	549	2400	628	370.0	300.2
8		C-b1r1d0	60	1	20	46.1	388	549	2400	628	300.5	326.0
9		C-b0r1d1	60	1	20	46.1	388	549	2400	628	386.1	449.0
10		C-b1r1d1	60	1	20	46.1	388	549	2400	628	461.1	547.0
11	Zhao [18]	S45-P10-C65u	45	2	16	51.1	400	540	3800	942	492.4	493.0
12		S60-P10-C40	60	2	20	32.6	400	540	3800	942	801.4	1033.5
13		S60-P10-C55	60	2	20	44.4	400	540	3800	942	977.5	1130.0
14		S60-P10-C65	60	2	20	51.1	400	540	3800	942	955.6	1101
15		S60-P8-C65	60	2	20	51.7	400	540	3800	603	1055.8	1087.5
16		S80-P10-C65	80	2	25	53.0	400	540	3800	942	1443.6	1527

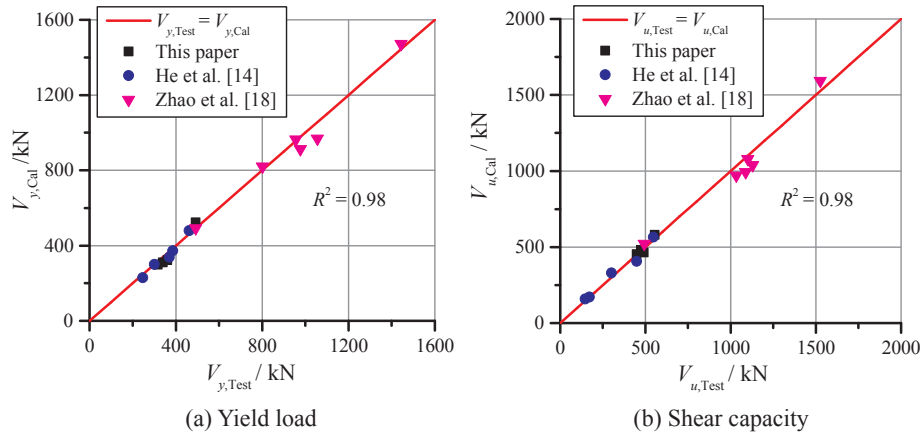


Fig. 21. Validation of equations.

R^2 equals 0.98.

5.3. Shear capacity equations

According to test results and existing equations, the shear bearing capacity of perfobond connectors possibly consists of the contributions of concrete dowels, perforated rebars, transverse reinforcements and bond forces. The failure modes of majority existing modified push-out tests are the shear fractures of perforated rebars, accompanied with more than 10 mm ultimate slips. Also, shear fracture planes form at concrete dowels and slip along the surface of steel plates. Although the shear resistance of concrete dowels decreases with the sliding, there remains the mechanical frictional force on fracture planes. Referred to the test results of specimen C-b0r0d1 and C-b1r0d1 from He et al. [14], the shear capacity reduction factor for concrete dowels at the ultimate bearing state is taken as 0.75.

Based on the parametric study results in Table 3, RPBLs with different thickness rubber rings have close ultimate shear capacities. The reason is that the rubber rings diminish the internal friction actions of fractured concrete dowels at the ultimate bearing stage. Concrete dowels make negligible contributions to the ultimate shear capacity in perfobond connectors with rubber rings so that the reduction factor for concrete dowels equals 0.

Since less cracking of concrete blocks happens in modified push-out tests, compared with ordinary push-out tests, the shear capacity of perforated rebars can be sufficiently realized. It is noted that the failure mode of perforated rebars is similar to that of headed stud connectors. Eurocode 4 [22] utilizes the tensile strength and the coefficient 0.8 to calculate the shear bearing capacity of headed stud connectors. Therefore, the contribution of perforated rebars on shear capacity is calculated by the product of tensile strength and cross-section area. The coefficient is determined as 1.58, which is identical to that in the yield load equations and approximate two times the coefficient used for headed studs.

As slips rise, the concrete in holes expands and the transverse reinforcements in tension make concrete blocks clamp steel plates, i.e., the expansion-clamping action. The expansion-clamping effect of transverse reinforcements is taken into account in the shear capacity equations, while the contributions of bonds are ignored at large slips. Since cracks perpendicular to transverse reinforcements occurred at concrete block surfaces in tests, it is assumed that the transverse reinforcements had yielded when the specimens were loaded to the ultimate shear capacity. Due to large shear deformation and complex force state, the expansion-clamping effect of perforated rebars is ignored. Referring to Eq. (14), the frictional coefficient is taken as 0.65.

According to the analysis above, the shear capacity equations for PBLs and RPBLs are proposed as Eqs. (18) and (19). Similarly, the

calculated results are compared with the collected test results, as shown in Table 6 and Fig. 21(b). The mean and maximum errors are 0.1% and 10.1%. For each series of tests, the mean errors are 2.2%, 2.4% and -2.4%, respectively. The determination coefficient equals 0.98.

$$V_u = 1.32\alpha_A A_c f_c n + 1.58 A_s f_u n + 0.65 A_{tr} f'_y \quad (18)$$

$$V_{u,rub} = 1.58 A_s f_u n + 0.65 A_{tr} f'_y \quad (19)$$

6. Conclusion

This paper carried out four modified push-out tests to study the shear behavior of rubber-ring perfobond connectors. The failure modes, load-slip curves, load-strain curves on steel plates and perforated rebars were analyzed. Further, three-dimensional nonlinear FEA models of modified push-out tests were built and validated by the test results. The shear mechanism of each component and the effects of rubber ring thickness on shear behaviors were discussed. Finally, based on the test results from this paper and references, the yield load equation and shear capacity equation of rubber-ring perfobond connectors with acceptable accuracy were proposed. The following conclusions could be drawn:

- (1) Compared with ordinary perfobond connectors, the yield slip of specimens with 2 mm, 4 mm and 6 mm thick rubber rings increases by 304%, 509% and 745%. This indicates that the rubber rings can significantly boost the slipping ability of perfobond connectors and improve uneven shear distributions in connector groups.
- (2) Based on the FEA parametric study, the perfobond connectors with different thickness of rubber rings have close ultimate shear capacities, while the yield loads significantly decrease with the growth of rubber ring thickness. Since the rubber rings diminish the confinement of surrounding concrete, a linear reduction factor for different rubber ring thicknesses on the contribution of concrete dowels was put forward.
- (3) By analyzing the existing equations, the yield load consists of the contributions of concrete dowels, perforated rebars and bond forces; while the shear bearing capacity involves concrete dowels, perforated rebars and transverse reinforcements. The yield load and shear capacity equations of perfobond connectors with or without rubber rings were proposed. The calculated results are in good agreement with the test results from this paper and references.

This paper focused on the basic shear behavior of RPBLs. Modified push-out test results of multi-hole specimens with rubber rings on partial holes will be discussed in the next phase.

References

- [1] Liu Y, Xin H, He J. Experimental and analytical study on fatigue behavior of composite truss joints. *J. Constr. Steel Res.* 2013;83(2):21–36.
- [2] Liu Y, Xin H, Liu Y. Load transfer mechanism and fatigue performance evaluation of suspender-girder composite anchorage joints at serviceability stage. *J. Constr. Steel Res.* 2018;145:82–96.
- [3] Oguejiofor EC, Hosain MU. A parametric study of perfbond rib shear connectors. *Can J Civ Eng* 1994;21(4):614–25.
- [4] Hosaka T, et al. An experimental study on shear characteristics of perfbond strip and its rational strength equations. *J Struct Eng* 2000;46:1593–604.
- [5] Ahn J, Lee C, Won J. Shear resistance of the perfbond-rib shear connector depending on concrete strength and rib arrangement. *J Constr Steel Res* 2010;66(10):1295–307.
- [6] Zheng S, Liu Y, Yoda T. Parametric study on shear capacity of circular-hole and long-hole perfbond shear connector. *J Constr Steel Res* 2016;117:64–80.
- [7] Allahyari H, Nikbin IM, Saman RR, et al. A new approach to determine strength of Perfbond rib shear connector in steel-concrete composite structures by employing neural network. *Eng Struct* 2018;157:235–49.
- [8] Yamadera N, Itoh N, Morikawa H. Design of the Tsurumi fairway bridge. *Bridge Foundation Eng* 1993;2(2):23–32. (in Japanese).
- [9] Wang Z, Li Q, Zhao C. Ultimate shear resistance of perfbond rib shear connectors based on a modified push-out test. *Adv Struct Eng* 2013;16(4):667–80.
- [10] Su Q, Wang W, Luan H. Experimental research on bearing mechanism of perfbond rib shear connectors. *J Constr Steel Res* 2014;95:22–31.
- [11] Su Q, Yang G, Bradford MA. Bearing capacity of perfbond rib shear connectors in composite girder bridges. *J Bridge Eng* 2016;21(4):06015009.
- [12] Zhang Q, Li Q, Tang L. Fracture mechanism and ultimate carrying capacity of shear connectors applied for steel-concrete joint segment of bridge pylon. *China J Highway Transport* 2007;20(1):85–90. (in Chinese).
- [13] Wang W, Zhao C, Li Q. Study on load-slip characteristic curves of perfbond shear connectors in hybrid structures. *J Adv Concr Technol* 2014;12(10):413–24.
- [14] He S, Fang Z. Experimental study on perfbond strip connector in steel–concrete joints of hybrid bridges. *J Constr Steel Res* 2016;118:169–79.
- [15] He S, Fang Z, Mosallam A. Push-out tests for perfbond strip connectors with UHPC grout in the joints of steel-concrete hybrid bridge girders. *Engr. Struct.* 2017;135:177–90.
- [16] Nakajima A, Nguyen MH. Strain behavior of penetrating rebar in perfbond strip and its evaluation of shear resistance. *J JSCE* 2016;4(1):1–18.
- [17] Xiao L, Li X, Ma Z. Behavior of perforated shear connectors in steel-concrete composite joints of hybrid bridges. *J Bridge Eng* 2016;22(4):04016135.
- [18] Zhao C, Li Z, Deng K. Experimental investigation on the bearing mechanism of Perfbond rib shear connectors. *Eng Struct* 2018;159:172–84.
- [19] Zhang Q, Pei S, Cheng Z. Theoretical and experimental studies of the internal force transfer mechanism of perfbond rib shear connector group. *J Bridge Eng* 2016;22(2):04016112.
- [20] Xu X, Liu Y, He J. Study on mechanical behavior of rubber-sleeved studs for steel and concrete composite structures. *Constr Build Mater* 2014;53:533–46.
- [21] Xu X, Liu Y. Analytical and numerical study of the shear stiffness of rubber-sleeved stud. *J Constr Steel Res* 2016;123:68–78.
- [22] EUROCODE 4, EN 1994-1-1, Design of Composite Steel and Concrete Structures Part 1.1 General Rules and Rules for Buildings, CEN-European Committee for Standardization, Brussels (2005).
- [23] ABAQUS Documentation. Version 6.12. Dassault system, USA (2012).
- [24] Lubliner J, Oliver J, Oller S. A plastic-damage model for concrete. *Int J Solids Struct* 1989;25(3):299–326.
- [25] Lee J, Fenves GL. Plastic-damage model for cyclic loading of concrete structures. *J Eng Mech* 1998;124(8):892–900.
- [26] Schickert G, Winkler H. Results of test concerning to multi-axial compressive stresses. Berlin Germany: Deutscher Ausschuss für Stahlbeton; 1977.
- [27] Richart FE, Brandtæg A, Brown RL. A study of the failure of concrete under combined compressive stresses. University of Illinois Engineering Experiment Station, Urbana; 1982.
- [28] Mills LL, Zimmerman RM. Compressive strength of plain concrete under multiaxial loading conditions. *J American Concrete Inst* 1970;66.
- [29] CEB-FIP Model Code 2010, British Standard Institution (2010).
- [30] Nguyen HT, Kim SE. Finite element modeling of push-out tests for large stud shear connectors. *J. Constr. Steel Res.* 2009;65(10–11):1909–20.
- [31] Comite Euro-International du Béton, Bulletin D'information No. 213/214. CEB-FIP Model Code 1990 (Concrete Structures), Lausanne, (1993).
- [32] Hordijk DA. Tensile and tensile fatigue behaviour of concrete; experiments, modelling and analyses. Heron 1992;37.
- [33] Brunesi E, Nascimbene R. Numerical web-shear strength assessment of precast prestressed hollow core slab units. *Eng Struct* 2015;102:13–30.